Biogeosciences
Open Access
Discussions

Photooxidation of dimethylsulfide (DMS) in the Canadian Arctic

A. Taalba[1], H. Xie[1], M. G. Scarratt[2], S. Bélanger[3], and M. Levasseur[4]

[1]Institut des sciences de la mer de Rimouski, Université du Québec à Rimouski, Rimouski, Québec, G5L 3A1, Canada
[2]Maurice Lamontagne Institute, Fisheries and Oceans Canada, Mont-Joli, Quebec, G5H 3Z4, Canada
[3]Département de biologie, chimie et géographie, Université du Québec à Rimouski, Rimouski, Québec, G5L 3A1, Canada
[4]Département de biologie (Québec–Océan), Universitè Laval, Québec, Québec, G1V 0A6, Canada

Correspondence to: H. Xie (huixiang_xie@uqar.qc.ca)

Discussion Paper | Discussion Paper | Discussion Paper | Discussion Paper

BGD

10, 2093–2126, 2013

Photolysis of DMS in the Arctic

A. Taalba et al.

Title Page

Abstract | Introduction

Conclusions | References

Tables | Figures

|◀ | ▶|

◀ | ▶

Back | Close

Full Screen / Esc

Printer-friendly Version

Interactive Discussion

Abstract

Photolysis of dimethylsulfide (DMS), a secondary photochemical process mediated by chromophoric dissolved organic matter (CDOM), has previously been demonstrated to be an important loss term of DMS in the surface layer of warm seas and the Southern Ocean. The role of photolysis in regulating the DMS dynamics in the Arctic Ocean, however, remains obscure. This study for the first time determined the apparent quantum yield (AQY) spectra of DMS photooxidation in northern polar marine milieus covering the Baffin Bay in the eastern Canadian Arctic and the Mackenzie River estuary, Mackenzie Shelf and Canada Basin in the western Canadian Arctic. The DMS AQY was fairly invariant at salinities < 25 but rose rapidly with further increasing salinity, which is well defined by a three-parameter exponential decay equation with a constant intercept. Salinity can therefore be used as a quantitative indicator of the DMS AQY. The DMS AQY in the ultraviolet (UV) wavelengths was linearly and positively correlated with the spectral slope coefficient (275–295 nm) of the CDOM absorption spectrum, suggesting that marine CDOM photosensitizes the degradation of DMS more efficiently than does terrestrial CDOM. High concentrations of nitrate ($\sim 12\,\mu mol\,L^{-1}$) in deep water samples boosted DMS photooxidation by 70–80 %, due likely to radical chemistry of nitrate photolysis. Coupled optical-photochemical modeling, based on the obtained DMS AQY spectra, shows that UV-A (320–400 nm) accounted for 60–75 % of the DMS photolysis in the sunlit surface layer and that photochemistry degraded DMS on an e-folding time from 9 to 100 d (mean: 29 d). The photooxidation term on average accounted for 21 % of the DMS gross loss rate and was comparable to the atmospheric DMS ventilation rate estimated for the same geographic regions.

1 Introduction

Dimethylsulfide (DMS) is the most abundant volatile sulfur compound in seawater and its egress from the ocean accounts for ~ 50 % of the total biogenic sulfur flux to the

atmosphere (Bates et al., 1992; Liss et al., 1997). Upon entering the troposphere from the sea, DMS is rapidly oxidized to sulfate aerosols, contributing to the formation of cloud condensation nuclei (CCN). CNN increase cloud albedos and thus reduce solar radiation arriving at the earth's surface (Andreae and Crutzen, 1997). Marine DMS, along with other oceanic precursors (e.g. sea salts and organics) of atmospheric aerosols, may thus moderate climate warming (Charlson et al., 1987; Quinn and Bates, 2011). Moreover, the cycling of marine DMS and its precursor, dimethylsulfoniopropionate (DMSP), implicates a cascade of processes that impact not only the sulfur and carbon biogeochemistry but also the ecology and physiology of marine phytoplankton and bacteria (Kiene et al., 2000; Simó, 2004).

In contrast to the enormous progress made in mapping the concentrations and air-sea fluxes of DMS in major ocean basins (e.g. Kettle et al., 1999; Lana et al., 2011; Yang et al., 2011), our knowledge of DMS distributions and fluxes in Arctic seas remains rudimentary. Surface water DMS concentrations obtained from a limited number of Arctic field surveys are within ranges occurring in warmer oceans (Leck and Persson, 1996; Bouillon et al., 2002; Galí and Simó, 2010; Luce et al., 2011; Motard-Côté et al., 2012). Sharma et al. (1999) estimated that the efflux of DMS from the Arctic Ocean accounts for only 0.4 % of the world ocean's total flux but could have a significant effect on the regional cloud albedo. More recent works on Arctic DMS fluxes arrived at similar conclusions (Chang et al., 2011; Rempillo et al., 2011). Moreover, rising seawater temperatures and increasing open water areas (Comiso, 2006) in the Arctic Ocean are expected to promote primary production (hence DMS formation) and accelerate air-sea exchange. Model simulations predicted that the Arctic DMS emission rate will increase by 90 % if the atmospheric CO_2 level triples and totally ice-free conditions materialize in summer (Gabric et al., 2005).

The amount of seawater DMS available for transfer to the atmosphere is controlled by in situ production and loss processes in the surface ocean. DMS is generated biologically by phytoplankton and bacteria (Yoch, 2002; Stefels et al., 2007); it is lost by bacterial uptake (Kiene and Bates, 1990; Simó, 2004), photolysis (Brimblecombe

Photolysis of DMS in the Arctic

A. Taalba et al.

⏮ | ⏭

◀ | ▶

Back | Close

Full Screen / Esc

Printer-friendly Version

Interactive Discussion

and Shooter, 1986), and ventilation to the atmosphere. DMS photolysis is a secondary photochemical process induced by oxidants produced primarily from photoreactions of chromophoric dissolved organic matter (CDOM) (Brimblecombe and Shooter, 1986; Toole et al., 2003). Compared to concentration distributions and air-sea fluxes, even

5 less is known of the production and consumption rates of DMS in the Arctic, particularly for the photooxidation term. Like other CDOM photochemical processes, previous studies on DMS photooxidation in the Northern Hemisphere were predominantly restricted to low and mid-latitudes due partly to the logistic challenges of field surveys in the high north and partly to the implicit assumption that photochemistry is

10 irrelevant in the Arctic where low solar angles and extensive ice cover minimize the solar radiation available for aquatic photoprocesses (Amon and Meon, 2004). However, ongoing global changes appear to favor photoreactions in Arctic environments. First, Arctic climate warming shrinks ice extent and shortens ice cover period (Comiso, 2006), thereby allowing more solar energy to be passed into the water column. Sec-

15 ond, warming-induced melting of Arctic permafrost may increase the input of terrestrial CDOM to the Arctic Ocean (Retamal et al., 2008; Stedmon et al., 2011); CDOM is the primary substrate of marine photochemistry. Third, declining stratospheric ozone over the high northern latitudes leads to increasing ultraviolet (UV) radiation reaching the sea surface (Rex et al., 2004). Finally, strong surface water stratification in the Arctic

20 Ocean, which could be further intensified by growing freshwater runoff and ice melting, increases substrate exposure to solar radiation on a per-molecule basis. These factors combined together could synergistically enhance the photooxidation potential in the water column. Indeed, recent studies have observed significant photochemical CDOM transformation in the western Canadian Arctic under current ice conditions in

25 terms of carbon monoxide (Xie et al., 2009), carbon dioxide (Bélanger et al., 2006) and ammonium photoproduction (Xie et al., 2012). Modeling studies point to strengthened photooxidation under a totally ice-free scenario in the summer season (Bélanger et al., 2006; Xie et al., 2012).

Galí and Simó (2010) determined DMS photooxidation rates in waters off Green-land and concluded that photolysis and biological consumption rates are comparable within the upper mixed layer during summer. To our knowledge, this is to date the only published survey of DMS photooxidation in the Arctic Ocean. Here we report the first measurements of the pseudo-first-order apparent quantum yield (AQY) spectra of DMS photolysis in Arctic marine environments covering the Mackenzie estuary and shelf, Canada Basin, and Baffin Bay. We modeled the photochemical DMS turnover rate constants based on the obtained AQY spectra and discussed the implication of photooxidation for DMS cycling in northern marine systems.

2   Materials and methods

2.1   Sampling

Sampling was conducted aboard the icebreaker *CCGS Amundsen* in the southeast-ern (SE) Beaufort Sea in late June and July 2008 and in the Baffin Bay/Lancaster Sound area in September 2008 as part of the field campaigns for the 2007–2008 IPY's (International Polar Year) CFL (Circumpolar Flaw Lead system study) and Canadian Arctic SOLAS (Surface Ocean-Lower Atmosphere Study) programs. The SE Beaufort Sea was re-visited in August 2009 during the Mackenzie Light and Carbon (Malina) program (Fig. 1). The SE Beaufort Sea survey covered the Mackenzie River estuary (MRE), Mackenzie Shelf (MS), and Canada Basin (CB). Zodiac rafts were deployed during the Malina cruise to collect shallow waters in the MRE that included two salinity-gradient transects (SGTs): one in the east channel (SGT-E) covering stations from 391 to 398 and the other in the west channel (SGT-W) encompassing stations from 691 to 698. The eastern Canadian Arctic was sampled at three localities, Sta. 303 in the Lan-caster Sound and Sta. 126 and 140 in northeast Baffin Bay (Fig. 1). Only surface water samples (0–5 m) were collected except for Sta. 1526 at which three depths down to 950 m were sampled. SGT samples were taken with a clean high-density polyethylene

(HDPE) bucket and transferred into 10-L acid-cleaned HDPE jugs. Elsewhere, 12-L Niskin bottles mounted on a rosette sampler were employed. Salinity and water temperature were recoded using a SeaBird 911+ CTD (conductivity, temperature, depth) profiler. All samples were gravity-filtered upon collection through a Pall AcroPak 1000

5 filtration capsule sequentially containing 0.8- and 0.2-µm polyethersulfone membranes which had been thoroughly rinsed with Nanopure and sample water. Filtered water was transferred to acid-cleaned 4-L clear glass bottles and stored at 4 °C in darkness until further treatment in a land-based laboratory in Rimouski, Quebec. Detailed sampling information can be found in Table 1.

10 **2.2 Irradiation**

Prior to irradiation, water samples were re-filtered through 0.2-µm polyethersulfone membranes (PALL) and amended with an aqueous DMS stock solution to yield a final concentration of $\sim 10 \, \mathrm{nmol \, L^{-1}}$. Samples were then siphoned into pre-combusted quartz-windowed cells (ID: 3.4 cm; length: 11.4 cm) with clean Teflon tubing. The cell

15 was overflowed by twice its volume before being closed without headspace. The irradiation procedure followed that reported by Zhang et al. (2006) for determining carbon monoxide photoproduction. Briefly, samples in the quartz cells were irradiated in a temperature-controlled water bath (2–4 °C) under polychromatic radiation emitted from a SUNSET CPS solar simulator equipped with a 1.5-kW xenon lamp. To retrieve

20 DMS AQY spectra (see Sect. 2.4), eight light treatments were applied by screening the incident light through eight successive Schott long-band glass cutoff filters with model numbers of WG280, WG295, WG305, WG320, WG345, GG395, GG435 and GG495. The numeric values in the model numbers signify the nominal 50 % transmittance cutoff wavelengths. Spectral irradiance under each cutoff filter was measured at 1-nm incre-

25 ments from 250 nm to 700 nm using an Optronics OL-754 spectroradiometer outfitted with a fiber optic cable having a terminal Teflon diffuser and calibrated with an OL752-10E irradiance standard. Light exposure spanned 2.5 h for samples under shortwave cutoff filters (WG280, WG295, WG305, and WG320) and 4 h under long-wave cutoff

filters (WG345, GG395, GG435 and GG495). For each experiment, parallel dark controls were incubated to correct for any thermal loss of DMS.

2.3 Analysis

DMS in pre- and post-irradiation samples was concentrated with a purge-and-trap device and then quantified using a gas chromatograph (GC) (Varian 3400 or 3800) fitted with a pulsed flame photometric detector (GC-PFPD) (Scarratt et al., 2000). Briefly, samples were bubbled for 3 min with gaseous helium (60 mL min^{-1}) in a heated purging vessel (ca. 70 °C). The upper part of the vessel (15 cm long) was kept at 5 °C to reduce water vapor in the gas stream without condensation of DMS. A Pyrex drying tube containing calcium chloride removed residual water vapor in the gas stream exiting the purging vessel before a Teflon loop submerged in liquid nitrogen cryotrapped the DMS. The Teflon loop was then heated to ∼ 70 °C, releasing the trapped volatiles onto the GC column. The system was calibrated using a certified permeation tube source (Kin-Tek Laboratories) delivering DMS at 500 ng min^{-1}. The helium-diluted DMS stream from the permeation tube was passed through the purging apparatus and subjected to subsequent processing in the same manner as the samples. The quantification limit was 0.03 nmol L^{-1} based on 3 times the background noise. The precision of the method was better than 10 % (coefficient of variation).

CDOM absorbance in pre- and post-irradiation samples was measured at room temperature from 250 nm to 800-nm at 1-nm increments using a Perkin-Elmer Lambda 35 dual beam UV-visible spectrometer equipped with 10-cm quartz cuvettes and referenced to Nanopure water. The average absorbance over the 683–687-nm interval was subtracted as a background correction from the rest of the spectrum (Babin et al., 2003). Absorbance at wavelength λ (nm), $A_{\text{cdom},\lambda}$, was converted to absorption coefficient (base e), $a_{\text{cdom},\lambda}$ (m^{-1}), according to Eq. (1):

$$a_{\text{cdom},\lambda} = 2.303 A_{\text{cdom},\lambda} l^{-1} \tag{1}$$

where l is the path-length of the quartz cuvette (m).

Concentrations of nitrate in original samples, stored frozen at −80 °C, were determined using a Technicon III (Bran+Luebbe) Autoanalyzer with colorimetric methods adapted from Grasshoff et al. (1999).

2.4 Retrieval of AQY of DMS photooxidation

The spectral AQY of DMS photolysis, $\Phi_{dms,\lambda}$, is defined as the moles of DMS degraded per mole of photons absorbed by CDOM at wavelength λ. As a secondary photochemical reaction, DMS photolysis obeys pseudo-first-order kinetics (Brimblecombe and Shooter, 1986). Following the practice of Bouillon and Miller (2004, 2006), we define a pseudo-first-order AQY of DMS photolysis, $\Phi^*_{dms,\lambda}$ [m^3 (mol photons)$^{-1}$], which is $\Phi_{dms,\lambda}$ divided by DMS concentration ([DMS], moles m^{-3}). $\Phi^*_{dms,\lambda}$ is derived according to the protocol reported by Bouillon and Miller (2004, 2006). Briefly, the rate of DMS photolysis in an irradiation cell can be expressed by Eq. (2):

$$-\frac{d[DMS]}{dt} = [DMS]L^{-1}\int_{280}^{500} Q_{0,\lambda}\left[1 - \exp\left(-a_{cdom+w,\lambda}L\right)\right]\Phi^*_{dms,\lambda}d\lambda \tag{2}$$

where L is the path-length of the irradiation cell, $Q_{0,\lambda}$ the incident spectral photon flux (mol photons m^{-2} s^{-1} nm^{-1}), and $a_{cdom+w,\lambda}$ the sum of the absorption coefficients of CDOM and water ($a_{w,\lambda}$) (Pope and Fry, 1997; Buiteveld et al., 1994). Integrating the left-hand side of Eq. (2) from time zero ([DMS]$_0$) to t ([DMS]$_t$) arrives at Eq. (3):

$$\ln\left(\frac{[DMS]_0}{[DMS]_t}\right)t^{-1} = L^{-1}\int_{280}^{500} Q_{0,\lambda}\left[1 - \exp(-a_{cdom+w,\lambda}L)\right]\Phi^*_{dms,\lambda}d\lambda \tag{3}$$

All terms in Eq. (3) are known except $\Phi^*_{dms,\lambda}$, allowing $\Phi^*_{dms,\lambda}$ to to be derived using a statistical optimization approach originally proposed by Rundel (1983) and adapted

later by Xie et al. (1998) and Johannessen and Miller (2001). This approach assumes a known spectral shape (exponential decay) of $\Phi^*_{\text{dms},\lambda}$:

$$\Phi^*_{\text{dms},\lambda} = \Phi^*_{\text{dms},\lambda_{\text{ref}}} \exp\left[-S_{\Phi^*_{\text{dms}}}(\lambda - \lambda_{\text{ref}})\right] \tag{4}$$

$\Phi^*_{\text{dms},\lambda_{\text{ref}}}$ is $\Phi^*_{\text{dms},\lambda}$ at the reference wavelength (290 nm) and $S_{\Phi^*_{\text{dms}}}$ denotes the spectral slope coefficient representing the spectral shape of $\Phi^*_{\text{dms},\lambda}$. The pseudo-first-order DMS photolysis rate in an irradiation cell can then be predicted from Eq. (4) using the assumed function of $\Phi^*_{\text{dms},\lambda}$ with initial estimates of $\Phi^*_{\text{dms},\lambda_{\text{ref}}}$ and $S_{\Phi^*_{\text{dms}}}$. The optimum $\Phi^*_{\text{dms},\lambda_{\text{ref}}}$ and $S_{\Phi^*_{\text{dms}}}$ values were identified with a MATLAB-coded, iterative fit method by varying $\Phi^*_{\text{dms},\lambda_{\text{ref}}}$ and $S_{\Phi^*_{\text{dms}}}$ until the minimum residuals reached between the measured and predicted pseudo-first-order DMS photolysis rates for all samples from a single irradiation. The predicted rates agreed well with the measured ones with R^2 ranging from 0.943 to 0.996 (mean: 0.989, $n = 22$, Table 2).

2.5 Modeling photochemical turnover of DMS

The photochemical decay of [DMS] in the upper mixed layer, which was generally deeper than the euphotic zone, can be expressed by:

$$[\text{DMS}]_{\text{col,t}} = [\text{DMS}]_{\text{col,0}} \exp\left[-\left(Z_{\text{ml}}^{-1}\int_{290}^{500} Q_{\text{d,0}-,\lambda}\frac{a_{\text{cdom},\lambda}}{a_{t,\lambda}}\Phi^*_{\text{dms},\lambda}\text{d}\lambda\right)t\right] \tag{5}$$

$[\text{DMS}]_{\text{col,0}}$ and $[\text{DMS}]_{\text{col},t}$ are the depth-integrated DMS concentrations (i.e. column burden, $\mu\text{mol m}^{-2}$) at time zero and t (d), respectively. Z_{ml} denotes the upper mixed-layer depth (UMLD in m, Table 3), $Q_{\text{d,0}-,\lambda}$ is the downwelling solar photon flux just below the sea surface (mol photons $\text{m}^{-2}\,\text{d}^{-1}\,\text{nm}^{-1}$), and $a_{t,\lambda}$ is the total absorption coefficient (m^{-1}), i.e. $a_{t,\lambda} = a_{\text{cdom},\lambda} + a_{\text{p},\lambda} + a_{\text{w},\lambda}$ where $a_{\text{p},\lambda}$ is the absorption coefficient of total

2101

Full Screen / Esc

Printer-friendly Version

Interactive Discussion

particulate matter. $Q_{d,0-,\lambda}$ was derived from model simulations at 3 h intervals using the Santa Barbara DISORT Atmospheric Radiative Transfer (SBDART) software (Ricchiazzi et al., 1998), accounting for the cloud cover and ozone conditions. Values of simulation parameters such as cloud fraction, cloud optical thickness, and ozone abundance were obtained from the International Satellite Cloud Climatology Project website (http://isccp.giss.nasa.gov/products/browsed2.html). Readers are referred to the study by Song et al. (2012) for the methodology of particle absorption measurement and for the Malina $a_{p,\lambda}$ data. The exponent in Eq. (5) is the photolysis rate constant, k_{dms} (d^{-1}), i.e.

$$k_{dms} = Z_{ml}^{-1} \int_{290}^{500} Q_{d,0-,\lambda} \frac{a_{cdom,\lambda}}{a_{t,\lambda}} \Phi_{dms,\lambda}^* d\lambda \tag{6}$$

Note that Eq. (6) neglects backscattering of solar radiation to the atmosphere and assumes vertical homogeneity of [DMS], Φ_{dms}^* and absorption coefficients of various optical constituents in the upper mixed layer. Daily averaged $Q_{d,0-,\lambda}$ value on each station's sampling date was used to calculate k_{dms}.

3 Results and discussion

3.1 General physical and chemical properties

The CFL stations covered the most extensive ranges of salinity (0–34.87) and water temperature (−1.5–14.9 °C) and represented the overall ranges of the entire datasets of the two parameters (Table 1). The temperature and salinity profiles of Sta. 1562 (not shown) indicate that the 5-m sample was within the upper polar mixed layer characterized by relatively low salinities caused by ice melting and runoff, the 160-m sample was located in the upper halocline formed by Pacific winter water, and the 950-m sample

originated from the North Atlantic (Matsouka et al., 2012). The Malina cruise encountered surface water temperature ranging from −0.8 °C (Sta. 320) to 10.3 °C (Sta. 697) and salinity spanning from 0.15 (Sta. 697) to 27.82 (Sta. 391) (Table 1). Evidently, water temperature during both CFL and Malina declined from the MRE to MS to CB and salinity climbed from the MRE to MS. However, Sta. 320, 640 and 1526 in the CB exhibited lower salinities than did certain stations on the MS (e.g. Sta. 320 vs. Sta. 391; Sta. 640 vs. Sta. 670 and 691; Sta. 1526 vs. Sta. 434), due probably to a stronger presence of ice meltwater in the CB in summer (Xie et al., 2012). The three stations visited during SOLAS in the eastern Canadian Arctic displayed little variation in surface water temperature (0.3–3.6 °C) and salinity (30.88–31.59). These thermohaline properties reflected the influence of the Pacific water flowing from the western Canadian Arctic to the Baffin Bay through the Canadian Archipelago (Melling, 2000).

The CDOM absorption coefficient along the Malina's two SGTs showed linear anti-correlations with salinity (Fig. 2). CDOM across the SGTs was thus mainly controlled by conservative mixing. Sta. 697 was an exception having $a_{\mathrm{cdom,412}}$ of 20 % lower than extrapolated from the $a_{\mathrm{cdom,412}}$–salinity regression line for the SGT-W, implying CDOM input near the head of the west channel of the MRE. CDOM in the east channel of the MRE was consistently higher than in the west channel, suggesting either a higher CDOM end member in the east channel of the river or a larger CDOM addition at the start of estuarine mixing in the east. The zero salinity sample from CFL (Sta. S0) was only slightly higher in $a_{\mathrm{cdom,412}}$ than the near-zero sample from Malina (Sta. 697) in spite of different sampling seasons (late June 2008 vs. mid-August 2009) and location (east vs. west channel). The ice meltwater-diluted surface water at Sta. 640 and 1526 showed lower $a_{\mathrm{cdom,412}}$ than expected from salinity, congruent with a previous finding that meltwater is deprived of CDOM (Matsouka et al., 2012). The subsurface samples at Sta. 1526, regardless of Pacific or Atlantic origin, were enriched with CDOM relative to their salinities. The CDOM absorption values of the three Baffin Bay stations conformed to the $a_{\mathrm{cdom,412}}$–salinity trend for the SE Beaufort Sea, which is in line with the

eastward transport pathway of the surface water in the western Canadian Arctic, as mentioned earlier.

3.2 AQY and action spectra of DMS photooxidation

Fitted parameters of Eq. (4) for deriving Φ^*_{dms} are shown in Table 2 and examples of Φ^*_{dms} spectra are displayed in Fig. 3. Φ^*_{dms} spectra representative of the MRE (Sta. 697), MS (Sta. 691), and CB (Sta. 640) indicate that Φ^*_{dms} increased from inshore to offshore with the difference climbing toward the short wavelengths (Fig. 3d). The surface action spectra were calculated as the products of Φ^*_{dms}, $Q_{surf,\lambda}$ (Fig. 3a) and $a_{cdom,\lambda}$ (Fig. 3b), where $Q_{surf,\lambda}$ (mol photons m^{-2} s^{-1} nm^{-1}) denotes the surface spectral solar photon flux at 70° N, 133° W and 14:00 local time on 1 July, simulated using the SMARTS model (Gueymard, 2001) under mid-summer Arctic atmospheric and cloudless conditions with an ozone column burden of 330 Dobson units. The spectra show a non-Gaussian shape, peaking at $\sim$ 330 nm and slightly tailing into the visible (Fig 3e). Despite Φ^*_{dms} being higher at the offshore Sta. 640, its surface action spectrum was well below that for the inshore Sta. 697 due to the highly elevated CDOM abundance in the estuarine water (Fig. 3b). The depth-integrated action spectra were computed as products of Φ^*_{dms}, $Q_{surf,\lambda}$ and $a_{cdom,\lambda}/a_t$. Their shapes resembled those of the surface action spectra but were more shifted toward the visible because of the deeper penetration into the water column by visible wavelengths as compared with UV. Contrasting with the surface action spectra, the depth-integrated action spectra of Sta. 640 and 691 lay far above that of Sta. 697, where particles contributed a lot more to the total absorption than at the other two stations (Song et al., 2012), hence leading to a much lower a_{cdom}/a_t ratio (Fig. 3c). The relative contributions of UV-B (290–320 nm), UV-A (320–400 nm), and visible (400–500 nm) to the full-spectrum DMS photolysis were assessed by integrating the spectral curves in Fig. 3e, f over the relevant wavelength ranges. Estimates indicate that UV-B, UV-A, and visible, respectively, contributed $\sim$ 10–20 %, $\sim$ 75 %, and $\sim$ 4–15 % at the surface and $\sim$ 5–15 %, $\sim$ 60–75 %, and $\sim$ 10–35 %

on a depth-integrated basis. UV-A thus dominated DMS photolysis both at the surface and in the entire water column, which is consistent with the results reported for warmer waters (Kieber et al., 1996; Toole et al., 2003, 2004; Bouillon et al., 2006).

Scatter plots of Φ^*_{dms} against salinity, pooling data from all three cruises, indicate Φ^*_{dms} in the UV regime remained rather constant below salinity 25 but increased rapidly above salinity 30, which can be described by a 3-parameter exponential form having a constant intercept (Fig. 4a, b). It is interesting to note that data from warmer seas, including the Sargasso Sea, NE Pacific, Bering Sea, and Lower St. Lawrence estuary, also nicely fit this trend. This characteristic pattern, nevertheless, became obscure across the visible wavelengths (Fig. 4c). Salinity can thus be used potentially as a cross-system indicator of Φ^*_{dms} within the UV spectral range, which, if confirmed in the future, lays a basis for modeling DMS photolysis rates on large spatial scales. Since a_{cdom} was approximately anti-correlated with salinity (Fig. 2), the $\Phi^*_{dms} - a_{cdom}$ relationship roughly mirrored that of Φ^*_{dms}-salinity but with relatively lower R^2 (data not shown).

Although increasing ionic strength (hence salinity) has been alluded to favor DMS photolysis (Yang et al., 2007), the dominant factor controlling this photoprocess in natural waters is thought to be CDOM, which indirectly oxidizes DMS via photoproduction of reactive oxygen species, such as singlet oxygen, hydroxyl radicals, and superoxide radicals (Brimblecombe and Shooter, 1986; Toole et al., 2004). As offshore waters are less impacted by terrestrial runoff in which CDOM is usually enriched with aromatic moieties relative to marine CDOM (Benner, 1998 and references therein), the striking difference in Φ^*_{dms} between low- and high-salinity samples (Fig. 4) might result from differing photosensitizing capacities of terrestrial and marine CDOM with respect to DMS photooxidation. To further confirm this proposition, Φ^*_{dms} is plotted against the spectral slope coefficient of CDOM over the wavelength range from 275 nm to 295 nm ($S_{275-295}$). $S_{275-295}$ has been proven to be a tracer of terrigenous dissolved organic matter with lower $S_{275-295}$ values indicating higher contents of land-derived materials (Fichot and Benner, 2012). Figure 5 manifests that Φ^*_{dms} increased with rising $S_{275-295}$,

linearly in the UV domain and exponentially across the visible span. Notwithstanding photobleaching can raise $S_{275-295}$ (Helms et al., 2008; Fichot and Benner, 2012), the generally conservative behavior of CDOM (Sect. 3.1; also see Xie et al., 2012) suggests that photobleaching should not be an important factor controlling $S_{275-295}$ in the
5 study area. Therefore, it appears that marine CDOM, which is rich in alkyl carbons (Benner, 1998), photosensitized the oxidation of DMS more efficiently than aromatic carbon-dominated terrigenous CDOM on an absorbed-photon basis. This is somewhat counter-intuitive, since aromatic-rich CDOM is considered to be more photoreactive in general (Zepp, 2003). Further investigations employing model terrestrial and marine
10 humic substances are needed to elucidate the underlying mechanism.

Note that the Φ^*_{dms} values at the UV wavelengths for the deep samples (160 m and 950 m) at Sta. 1526 in the CB strayed far upward from the $\Phi^*_{dms} - S_{275-295}$ trendlines (Fig. 5a, b). These elevated Φ^*_{dms} values are consistent with the much higher concentrations of nitrate observed at the deeper depths ($\sim 12\,\mu\text{mol}\,\text{L}^{-1}$, Table 1). Photolysis
15 of nitrate has been identified as an alternative route for DMS photooxidation in nitrate-rich natural waters (Bouillon and Miller, 2004; Toole et al., 2004). The enhancement of DMS photooxidation in the presence of nitrate is ascribed to the production of DMS-oxidizing $\text{HO}^\bullet$ (directly) and $\text{B}^\bullet_2$ (indirectly) radicals from nitrate photolysis (Bouillon and Miller, 2005). The relationship between $\Phi^*_{dms,330}$ and nitrate concentration reported by
20 Bouillon and Miller (2004) indicates that nitrate photolysis can account for 81 % of the DMS photooxidation at a nitrate concentration of $12\,\mu\text{mol}\,\text{L}^{-1}$. The $\Phi^*_{dms,330}$ values for the deep samples at Sta. 1526 are 72 % to 81 % higher than those expected from the $\Phi^*_{dms,330} - S_{275-295}$ regression line (Fig. 5b), broadly agreeing with the prediction of Bouillon and Miller (2004). The absence of the nitrate enhancement effect in the vis-
25 ible (Fig. 5c) conforms to the fact that nitrate only absorbs short UV radiation (Mack and Bolton, 1999). The nitrate concentrations in surface samples having salinity ≥ 15 were very low (undetectable to $0.7\,\mu\text{mol}\,\text{L}^{-1}$, Table 1), leading to negligible effects on DMS photolysis. The low-salinity (0–9.43) estuarine samples, though having moderate nitrate levels (1.79–$3.62\,\mu\text{mol}\,\text{L}^{-1}$, Table 1), showed no perceptible nitrate influence,

either. This could be attributed to the low concentrations of the bromide anion in fresh-water, since the bromide anion plays a key role in the nitrate-induced photooxidation of DMS, particularly in solutions of low dissolved inorganic carbon concentrations (Bouillon and Miller, 2005).

3.3 Photochemical turnover of DMS

The photochemical turnover rate constants (k_{dms}) in the surface mixed layer estimated from Eq. (6) for each sampling station are displayed in Table 3, along with the parallel $a_{cdom,330}/a_{t,330}$ ratios, UMLDs, and daily integrated downwelling solar irradiances just beneath the sea surface. Equation (6) indicates that k_{dms} is positively related to Φ^*_{dms}, the a_{cdom}/a_t ratio and solar irradiance but is inversely proportional to the surface mixed layer depth. Data of k_{dms} pooled from all three field surveys ranged from 0.01–0.11 d^{-1} and averaged 0.034 d^{-1} with a standard deviation of 0.022 d^{-1}. The highest k_{dms} (0.11 d^{-1}) occurred at Sta. 391 with relatively large DMS AQYs [$\Phi^*_{dms,330}$: 0.30 m^3 (mol photons)$^{-1}$], moderately high a_{cdom}/a_t ratios (0.87 at 330 nm), and a shallow mixed layer (4.0 m) while one of the two lowest rate constants (0.01 d^{-1}) was observed at Sta. 170 having smaller AQYs [$\Phi^*_{dms,330}$: 0.2 m^3 (mol photons)$^{-1}$], lower a_{cdom}/a_t ratios (0.66 at 330 nm), and a much deeper mixed layer (11.5 m). The other lowest k_{dms} appeared at Sta. 1526 at which the positive effect of strong solar radiation (19.3 mol photons m^{-2} d^{-1}) and high a_{cdom}/a_t ratios (0.93 at 330 nm) was overtaken by the negative effect of deep mixing (19.0 m) and a sharply titled AQY spectrum ($S_{\Phi^*_{dms}}$: 0.063 nm^{-1}). Per subdivision, the Mackenzie Shelf, including the two estuarine transects, on average exhibited the most elevated k_{dms} (mean ± s.d.: 0.038 ± 0.025 d^{-1}) followed by the Baffin Bay (0.027±0.004 d^{-1}) and the Canada Basin (0.018±0.010 d^{-1}). Clearly, despite the lower AQYs [$\Phi^*_{dms,330}$: 0.13±0.07 m^3 (mol photons)$^{-1}$] and a_{cdom}/a_t ratios (0.76 ± 0.19 at 330 nm) on the MS as compared to those in the CB ($\Phi^*_{dms,330}$: 0.26 ± 0.07 m^3 (mol photons)$^{-1}$; $a_{cdom,330}/a_{t,330}$: 0.94 ± 0.12) and Baffin Bay ($\Phi^*_{dms,330}$:

$0.68 \pm 0.20\,\mathrm{m}^3\,(\mathrm{mol\,photons})^{-1}$; $a_{\mathrm{cdom},330}/a_{\mathrm{t},330}$: 0.93), the far shallower mixed layer depth on the MS ($4.6 \pm 2.9\,\mathrm{m}$) led to k_{dms} surpassing those in the CB and Baffin Bay where the UMLD both averaged $\sim 14\,\mathrm{m}$.

The photochemical DMS turnover rate constants available in the literature vary by more than two orders of magnitude ($0.02\text{–}2.5\,\mathrm{d}^{-1}$). The rate constants from the present study are within the lower bounds of those previously reported (Table 4). In comparison with other high-latitude seas, our values are close to those observed in the Bering Sea ($0.02\text{–}0.11\,\mathrm{d}^{-1}$, Deal et al., 2005) and Ross Sea ($0.037\text{–}0.17\,\mathrm{d}^{-1}$, Del Valle et al., 2009) but much lower than the ones found in the Greenland Sea ($0.23\text{–}1.05\,\mathrm{d}^{-1}$, Galí and Simó, 2010) and northern Ross Sea ($0.5\text{–}0.71\,\mathrm{d}^{-1}$, Toole et al., 2004). Many factors could cause such large discrepancies, the most prominent ones being solar irradiance, DMS AQY, and UMLD. For example, the waters surveyed by Toole et al. (2004) were highly enriched in nitrate ($28.5\,\mu\mathrm{mol\,L}^{-1}$), giving rise to a $\Phi^*_{\mathrm{dms},330}$ of $4.7\,\mathrm{m}^3\,(\mathrm{mol\,photons})^{-1}$ according to the $\Phi^*_{\mathrm{dms},330}$-nitrate relationship proposed by Bouillon and Miller (2004). This $\Phi^*_{\mathrm{dms},330}$ is 20 times the average $\Phi^*_{\mathrm{dms},330}$ of our surface water samples [$0.23 \pm 0.22\,\mathrm{m}^3\,(\mathrm{mol\,photons})^{-1}$], which alone could explain the majority of the variability between the two studies. Note that previous studies often implicitly assumed all underwater light to be absorbed by dissolved chromophores without considering the particulate colored materials, which biased the k_{dms} estimates upward to a certain extent, depending on the fraction of light absorbed by particles. We made a correction for this bias by separating the light dose absorbed by CDOM from that by particles (Eq. 6), which was particularly relevant for particle-laden waters in the estuary and in the high-productivity upwelling zone nearby Cape Bathurst (Sta. 170, Song et al., 2012). Particles at these sites accounted for 30 % to 65 % of the total light absorption (Table 3). It should also be noted that Eq. (6) assumes vertically constant [DMS] in the mixed layer, which, albeit valid on a first-order approximation, tends to underestimate k_{dms} if [DMS] in the upper layer decreases with depth and vice versa.

Previous investigations have demonstrated that the photochemical route accounts for between 7% and 75% of the total DMS loss in the surface ocean (Kieber et al., 1996; Toole et al., 2003, 2004; Bouillon et al., 2006; Galí and Simó, 2010), thereby making an important contribution to the spatiotemporal variability of DMS concentrations in various oceanic environments. Under shallow stratification or nitrate-replete conditions, photolysis may even exceed bacterial uptake in DMS removal (Toole et al., 2004; Galí and Simó, 2010). There is currently a dearth of bacterial DMS consumption measurements in the Arctic Ocean. Limited data available indicate a large variability of bacterial DMS consumption turnover times in the upper mixed layer, ranging from ~ 1 d in the Greenland Sea (Galí and Simó, 2010) to ~ 3 d in the Barents Sea (Matrai and Vernet, 1997) to ~ 13 d in the central Arctic (Leck and Persson, 1996). Most of our photochemical DMS turnover times (i.e. $1/k_{dms}$, range: 9–100 d; mean: 29 d) are longer than even the slowest bacterial DMS uptake so far observed in the Arctic. Hence, photolysis of DMS is generally not expected to be the dominant loss term of this compound in Arctic seawater. There are no published bacterial DMS consumption data for the areas surveyed by the present study. However, the DMS turnover times with respect to microbial DMS production in these areas are known to range from 1 to 19 d and average 6 d (Luce et al., 2011), which are equivalent to the DMS gross loss turnover times (Kiene and Linn, 2000). Photooxidation thus on average accounts for 21% of the DMS gross loss term. Yet, the photochemical turnover times are similar in magnitude to the air-sea ventilation turnover times (Beaufort Sea: 2.2–57 d; Baffin Bay: 15–162 d); the latter were estimated using an UMLD of ~ 15 m (Table 3, excluding the two estuarine transects) and mixed-layer DMS concentrations (Beaufort Sea: $0.38\,\mathrm{nmol\,L^{-1}}$; Baffin Bay: $1.3\,\mathrm{nmol\,L^{-1}}$) and air-sea exchange fluxes (Beaufort Sea: $0.1\text{–}2.6\,\mathrm{\mu mol\,m^{-2}\,d^{-1}}$; Baffin Bay: $0.2\text{–}1.3\,\mathrm{\mu mol\,m^{-2}\,d^{-1}}$) collected from the same areas and seasons (Luce et al., 2011; Motard-Côté et al., 2012; Rempillo et al., 2011).

Lastly, all samples in the present study were taken in the summer and fall seasons when surface waters were depleted in nitrate except those within the Mackenzie River plume (Table 1). According to Tremblay et al. (2008), surface-water nitrate

concentrations in the coastal and offshore SE Beaufort Sea reach a maximum of $\sim 4 \, \mu mol \, L^{-1}$ in late April and early May when sea ice usually starts to break up. This level of nitrate would increase the DMS AQY by $\sim 50 \, \%$, translating to a $50 \, \%$ reduction in the photochemical DMS turnover time. Under otherwise similar conditions, the photochemical DMS turnover is thus expected to be faster in spring, i.e. on the order of $\sim 14 \, d$, which is comparable to the lower end of the biological DMS turnover estimates for the Arctic Ocean.

4 Summary

Salinity was identified as a good indicator of the DMS AQYs determined from estuarine, shelf, and open ocean waters in the Canadian Arctic. Surface water DMS AQY in the UV domain increased linearly with the spectral slope coefficient of CDOM, suggesting marine CDOM was more efficient than terrestrial CDOM at photosensitizing the decomposition of DMS. High DMS AQYs observed in nitrate-rich deep water samples were attributable to enhanced DMS degradation by radicals produced from nitrate photolysis. UV-A was the dominant spectral range of solar radiation responsible for DMS photooxidation both at the surface and on a depth-integrated basis. Coupled optical-photochemical modeling indicated that photochemical DMS turnover in the water column was controlled by diverse variables, among which the mixed-layer depth, AQY, solar irradiance, and the contribution of CDOM to the total underwater light absorption were the most important. Modeled photochemical DMS turnover times ranged from 9 to 100 d (mean: 29 d) and were similar to the atmospheric ventilation turnover times. It is suggested that the photochemical DMS turnover in spring could be twice as fast because of higher nitrate concentrations in surface water at the start of ice breakup.

References

Amon, R. M. W. and Meon, B.: The biogeochemistry of dissolved organic matter and nutrients in two large Arctic estuaries and potential implications for our understanding of the Arctic Ocean system, Mar. Chem., 92, 311–330, 2004.

Andreae, M. O. and Crutzen, P. J.: Atmospheric aerosols: biogeochemical sources and role in atmospheric chemistry, Science, 276, 1052–1058, 1997.

Babin, M., Stramski, D., Ferrari, G. M., Claustre, H., Bricaud, A., Obolensky, G., and Hoepffner, N.: Variations in the light absorption coefficients of phytoplankton, nonalgal particles, and dissolved organic matter in coastal waters around Europe, J. Geophys. Res., 108, 3211, doi:10.1029/2001JC000882, 2003.

Bates, T. S., Lamb, B. K., Guenther, A., Dignon, J., and Stoiber, R. E.: Sulfur emissions to the atmosphere from natural sources, J. Atmos. Chem., 14, 315–337, 1992.

Bélanger, S., Xie, H., Krotkov, N., Larouche, P., Vincent, W. F., and Babin, M.: Photomineralization of terrigenous dissolved organic matter in Arctic coastal waters from 1979 to 2003: interannual variability and implications of climate change, Global Biogeochem. Cy,, 20, GB4005, doi:10.1029/2006GB002708, 2006.

Bélanger, S., Babin, M., and Larouche, P.: An empirical ocean color algorithm for estimating the contribution of chromophoric dissolved organic matter to total light absorption in optically complex waters, J. Geophys. Res. 113, C04027, doi:10.1029/2007JC004436, 2008.

Benner, R. H.: Cycling of dissolved organic in the ocean, in: Aquatic Humic Substances: Ecology and Biogeochemistry, edited by: Hessen, D. O. and Tranvik, L. J., Springer-Verlag, Berlin, Germany, 317–331, 1998.

Bouillon, R.-C. and Miller, W. L.: Determination of apparent quantum yield spectra of DMS photo-degradation in an in situ iron-induced Northeast Pacific Ocean bloom, Geophys. Res. Lett., 31, L06310, doi:10.1029/2004GL019536, 2004.

Bouillon, R.-C. and Miller, W. L.: Photodegradation of dimethyl sulfide (DMS) in natural waters: laboratory assessment of the nitrate-photolysis-induced DMS oxidation, Environ. Sci. Technol., 39, 9471–9477, 2005.

Bouillon, R. C., Lee, P. A., de Mora, S. J., Levasseur, M., and Lovejoy C.: Vernal distribution of dimethylsulphide, dimethylsulphoniopropionate, and dimethylsulphoxide in the North Water in 1998, Deep-Sea Res. Pt. II, 49, 5171–5189, 2002.

Bouillon, R.-C., Miller, W. L., Levasseur, M., Scarratt, M., Merzouk, A., Michaud, S., Ziolkowski, L.: The effect of mesoscale iron enrichment on the marine photochemistry of dimethylsulfide in the NE subarctic Pacific, Deep-Sea Res. Pt. II, 53, 2384–2397, 2006.

Brimblecombe, P. and Shooter, D.: Photo-oxidation of dimethylsulphide in aqueous solution, Mar. Chem., 19, 343–353, 1986.

Brugger, A., Slezak, D., Obernosterer, I., and Herndl, G. J.: Photolysis of dimethylsulfide in the northern Adriatic Sea: dependence on substrate concentration, irradiance and DOC concentration, Mar. Chem., 59, 321–331, 1998.

Buiteveld, H., Hakvoort, J. M. H., and Donze, M.: The optical properties of pure water, in: SPIE Proceeding on Ocean Optics XII, edited by: Jaffe, J. S., The Society of Photo-Optical Instrumentation Engineers, 174–183, 1994.

Camill, P.: Permafrost thaw accelerates in boreal peatlands during late-20th century climate warming, Clim. Change, 68, 135–152, 2005.

Chang, R. Y.-W., Sjostedt, S. J., Pierce, J. R., Papakyriakou, T. N., Scarratt, M. G., Michaud, S., Levasseur, M., Leaitch, W. R., and Abbatt, J. P. D.: Relating atmospheric and oceanic DMS levels to particle nucleation events in the Canadian Arctic, J. Geophys. Res., 116, D00S03, doi:10.1029/2011JD015926, 2011.

Charlson, R. J., Lovelock, J. E., Andreae, M. O., and Warren, S. G.: Oceanic phytoplankton, atmospheric sulphur, cloud albedo and climate, Nature, 326, 655–661, 1987.

Comiso, J. C.: Abrupt decline in the Arctic winter sea ice cover, Geophys. Res. Lett., 33, L18504, doi:10.1029/2006GL027341, 2006.

Deal, C., Kieber, D., Toole, D., Stamnes, K., Jiang, S., and Uzuka, N.: Dimethylsulfide photolysis rates and apparent quantum yields in Bering Sea seawater, Cont. Shelf Res., 25, 1825–1835, 2005.

Photolysis of DMS in the Arctic

A. Taalba et al.

DelValle, D. A., Kieber, D. J., Toole, D. A., Brinkley, J., and Kiene, R. P.: Biological consumption of dimethylsulfide (DMS) and its importance in DMS dynamics in the Ross Sea, Antarctica, Limnol. Oceanogr., 54, 785–798, 2009.

Emmerton, C. A., Lesack, L. F. W., and Vincent, W. F.: Mackenzie River nutrient delivery to the Arctic Ocean and effects of the Mackenzie Delta during open water conditions, Global Biogeochem. Cy., 22, GB1024, doi:10.1029/2006GB002856, 2008.

Fichot, C. G. and Benner, R.: The spectral slope coefficient of chromophoric dissolved organic matter ($S_{275-295}$) as a tracer of terrigenous dissolved organic carbon in river-influenced ocean margins, Limnol. Oceanogr., 57, 1453–1466, 2012.

Gabric, A. J., Qu, B., Matrai, P., and Hirst, A. C.: The simulated response of dimethylsulfide production in the Arctic Ocean to global warming, Tellus B, 57, 391–403, doi:10.1111/j.1600-0889.2005.00163.x, 2005.

Galí, M. and Simó, R.: Occurrence and cycling of dimethylated sulfur compounds in the Arctic during summer receding of the ice edge, Mar. Chem., 122, 105–117, 2010.

Gueymard, C. A.: Parameterized transmittance model for direct beam and circumsolar spectral irradiance, Solar Energy, 71, 325–346, 2001.

Gunson, J. R., Spall, S. A., Anderson, T. R., Jones, A., Totterdell, I. J., and Woodage, M. J.: Climate sensitivity to ocean dimethylsulphide emissions, Geophys. Res. Lett., 33, L07701, doi:10.1029/2005GL024982, 2006.

Helms, J. R., Stubbins, A., Ritchie, J. D., Minor, E. C., Kieber, D. J., and Mopper, K.: Absorption spectral slopes and slope ratios as indicators of molecular weight, source, and photobleaching of chromophoric dissolved organic matter, Limnol. Oceanogr., 53, 955–969, 2008.

Hu, C., Muller-Karger, F. E., and Zepp, R. G.: Absorbance, absorption coefficient, and apparent quantum yield: a comment on common ambiguity in the use of these optical concepts, Limnol. Oceanogr., 47, 1261–1267, 2002.

Johannessen, S. C. and Miller, W. L.: Quantum yield for the photochemical production of dissolved inorganic carbon in seawater, Mar. Chem., 76, 271–283, 2001.

Kettle, A. J., Andreae, M. O., Amouroux, D., Andreae, T. W., Bates, T. S., Berresheim, H., Bingemer, H., Boniforti, R., Curran, M. A. J., DiTullio, G. R., Helas, G., Jones, G. B., Keller, M. D., Kiene, R. P., Leck, C., Levasseur, M., Malin, G., Maspero, M., Matrai, P., McTaggart, A. R., Mihalopoulos, N., Nguyen, B. C., Novo, A., Putaud, J. P., Rapsomanikis, S., Roberts, G., Schebeske, G., Sharma, S., Simo, R., Staubes, R., Turner, S., and Uher, G.: A global database of sea surface dimethylsulfide (DMS) measurements and a procedure to predict

sea surface DMS as a function of latitude, longitude, and month, Global Biogeochem. Cy., 13, 399–444, 1999.

Kieber, D. J., Jiao, J., Kiene, R. P., and Bates, T. S.: Impact of dimethylsulfide photochemistry on methyl sulfur cycling in the equatorial Pacific Ocean, J. Geophys. Res., 101, 3715–3722, 1996.

Kiene, R. P. and Bates, T. S.: Biological removal of dimethyl sulphide from sea water, Nature, 345, 702–705, 1990.

Kiene, R. P. and Linn, L. J.: The fate of dissolved dimethylsulfoniopropionate (DMSP) in seawater: tracer studies using ^{35}S-DMSP, Geochim. Cosmochim. Acta, 64, 2797–2810, 2000.

Kiene, R. P., Linn, L. J., and Bruton, J. A.: New and important roles for DMSP in marine microbial communities, J. Sea Res., 43, 209–224, 2000.

Lana, A., Bell, T. G., Simó, R., Vallina, S. M., Ballabrera-Poy, J., Kettle, A. J., Dachs, J., Bopp, L., Saltzman, E. S., Stefels, J., Johnson, J. E., and Liss, P. S.: An updated climatology of surface dimethlysulfide concentrations and emission fluxes in the global ocean, Global Biogeochem. Cy., 25, GB1004, doi:10.1029/2010GB003850, 2011.

Leck, C. and Persson, C.: The central Arctic Ocean as a source of dimethyl sulfide – seasonal variability in relation to biological activity, Tellus, Ser. B, 48, 156–177, 1996.

Liss, P. S., Hatton, A. D., Malin, G., Nightingale, P. D., and Turner, S. M.: Marine sulphur emissions, Philos. Trans. R. Soc. London, Ser. B, 352, 159–169, 1997.

Luce, M., Levasseur, M., Scarratt, M. G., Michaud, S., Royer, S.-J., Kiene, R., Lovejoy, C., Gosselin, M., Poulin, M., Gratton, Y., and Lizotte M.: Distribution and microbial metabolism of dimethylsulfoniopropionate and dimethylsulfide during the 2007 Arctic ice minimum, J. Geophys. Res., 116, C00G06, doi:10.1029/2010JC006914, 2011.

Mack, J. and Bolton, J. R.: Photochemistry of nitrite and nitrate in aqueous solution: a review, J. Photochem. Photobiol. A: Chem., 128, 1–13, 1999.

Matrai, P. A. and Vernet, M.: Dynamics of the vernal bloom in the marginal ice-zone of the Barents Sea: dimethyl sulfide and dimethylsulfoniopropionate budgets, J. Geophys Res. 102, 22965–22979, 1997.

Motard-Côté, J., Levasseur, M., Scarratt, M. G., Michaud, S., Gratton, Y., Rivkin, R. B., Keats, K., Gosselin, M., Tremblay, J.-É., Kiene, R. P., and Lovejoy, C.: Distribution and metabolism of dimethylsulfoniopropionate (DMSP) and phylogenetic affiliation of DMSP-assimilating bacteria in northern Baffin Bay/Lancaster Sound, J. Geophys. Res., 117, C00G11, doi:10.1029/2011JC007330, 2012.

Photolysis of DMS in the Arctic

A. Taalba et al.

Pope, R. M. and Fry, E. S.: Absorption spectrum (380–700 nm) of pure water. 2. Integrating cavity measurements, Appl. Opt., 36, 8710–8723, 1997.

Quinn, P. K. and Bates, T. S.: The case against climate regulation via oceanic phytoplankton sulphur emissions, Nature, 480, 51–56, 2011.

Rempillo, O., Seguin, A. M., Norman, A.-L., Scarratt, M., Michaud, S., Chang, R., Sjostedt, S., Abbatt, J., Else, B., Papakyriakou, T., Sharma, S., Grasby, S., and Levasseur, M.: Dimethyl sulfide air-sea fluxes and biogenic sulfur as a source of new aerosols in the Arctic fall, J. Geophys. Res., 116, D00S04, doi:10.1029/2011JD016336, 2011.

Retamal, L., Bonilla, S., and Vincent, W. F.: Optical gradients and phytoplankton production in the Mackenzie River and the coastal Beaufort Sea, Polar Biol., 31, 363–379, 2008.

Rex, M., Salawitch, R. J., von der Gathen, P., Harris, N. R. P., Chipperfield, M. P., and Naujokat, B.: Arctic ozone loss and climate change, Geophys. Res. Lett., 31, L04116, doi:10.1029/2003GL018844, 2004.

Ricchiazzi, P., Yang, S., and Gautier, C.: A practical tool for plane-parallel radiative transfer in the Earth's atmosphere, available at: http://arm.mrcsb.com/sbdart/html/sbdart-intro.html, 1998.

Scarratt, M., Cantin, G., Levasseur, M., and Michaud, S.: Particle size-fractionated kinetics of DMS production: where does DMSP cleavage occur at the microscale?, J. Sea Res., 43, 245–252, 2000.

Sharma, S., Barrie, L. A., Plummer, D., McConnell, J. C., Brickell, P. C., Levasseur, M., Gosselin, M., and Bates, T. S.: Flux estimation of oceanic dimethyl sulfide around North America, J. Geophys. Res., 104, 21327–21342, 1999.

Simó, R.: From cells to globe: approaching the dynamics of DMS(P) in the ocean at multiple scales, Can. J. Fish. Aquat. Sci., 61, 673–684, 2004.

Simó, R. and Pedrós-Alió, C.: Short-term variability in the open ocean cycle of dimethylsulfide, Global Biogeochem. Cy., 13, 1173–1181, 1999.

Six, K. D. and Maier-Reimer, E.: What controls the oceanic dimethylsulfide (DMS) cycle? A modeling approach, Global Biogeochem. Cy., 20, GB4011, doi:10.1029/2005GB002674, 2006.

Song, G., Xie, H., Bélanger, S., and Babin, M.: Spectrally resolved efficiencies of carbon monoxide (CO) photoproduction in the Western Canadian Arctic: particles versus solutes, Biogeosciences Discuss., 9, 16161–16211, doi:10.5194/bgd-9-16161-2012, 2012.

Stedmon, C. A. and Markager, S.: Behaviour of the optical properties of coloured dissolved organic matter under conservative mixing, Estuar. Coast. Shelf. Sci., 57, 973–979, 2003.

Stedmon, C. A., Amon, R. M. W., Rinehart, A. J., and Walker, S. A.: The supply and characteristics of colored dissolved organic matter (CDOM) in the Arctic Ocean: Pan Arctic trends and differences, Mar. Chem., 124, 108–118, 2011.

Stefels, J., Steinke, M., Turner, S., Malin, G., and Belviso, S.: Environmental constraints on the production and removal of the climatically active gas dimethylsulphide (DMS) and implications for ecosystem modelling, Biogeochemistry, 83, 245–275, 2007.

Toole, D. A., Kieber, D. J., Kiene, R. P., Siegel, D. A., and Nelson, N. B.: Photolysis and the dimethylsulfide (DMS) summer paradox in the Sargasso Sea, Limnol. Oceangr., 48, 1088–1100, 2003.

Toole, D. A., Kieber, D. J., Kiene, R. P., White, E. M., Bisgrove, J., del Valle, D. A., and Slezak, D.: High dimethyl sulfide photolysis rates in nitrate-rich Antarctic waters, Geophys. Res. Lett., 31, L11307, doi:10.1029/2004GL019863, 2004.

Toole, D. A., Slezak, D., Kiene, R. P., Kieber, D. J., and Siegel, D. A.: Effects of solar radiation on dimethylsulfide cycling in the western Atlantic Ocean, Deep-Sea Res. Pt. I, 53, 136–153, 2006.

Tremblay, J.-É, Simpson, K., Martin, J., Miller, L., Gratton, Y., Barber, D., and Price, N. M.: Vertical stability and the annual dynamics of nutrients and chlorophyll fluorescence in the coastal, southeast Beaufort Sea, J. Geophys. Res., 113, C07S90, doi:10.1029/2007JC004547, 2008.

Twardowski, M. S., Boss, E., Sullivan, J. M., and Donaghay, P. L.: Modeling the spectral shape of absorption by chromophoric dissolved organic matter, Mar. Chem., 89, 69–88, 2004.

Vallina, S. M. and Simó, R.: Strong relationship between DMS and the solar radiation dose over the global surface ocean, Science, 315, 506–508, 2007.

Xie, H., Moore, R. M., and Miller, W. L.: Photochemical production of carbon disulphide in seawater, J. Geophys. Res., 103, 5635–5644, 1998.

Xie, H., Bélanger, S., Demers, S., Vincent, W. F., and Papakytiakou, T. N.: Photobiogeochemical cycling of carbon monoxide in the southeastern Beaufort Sea in spring and autumn, Limnol. Oceanogr., 54, 234–249, 2009.

Yang, G.-P., Li., C., Qi, J., Hu, L., and Hou, H.: Photochemical oxidation of dimethylsulfide in seawater, Acta Oceanol. Sin., 26, 34–42, 2007.

Title Page

Abstract | Introduction

Conclusions | References

Tables | Figures

|◀ | ▶|

◀ | ▶

Back | Close

Full Screen / Esc

Printer-friendly Version

Interactive Discussion

Yang, G.-P., Zhang, H.-H., Zhou, L.-M., and Yang, J.: Temporal and spatial variations of dimethylsulfide (DMS) and dimethylsulfoniopropionate (DMSP) in the East China Sea and the Yellow Sea, Cont. Shelf Res., 31, 1325–1335, 2011.

Yoch, D. C.: Dimethylsulfoniopropionate: its sources, role in the marine food web, and biological degradation to dimethylsulfide, Appl. Environ. Microbiol., 68, 5804–5815, 2002.

Zemmelink, H. J., Dacey, J. W. H., Hintsa, E. J., McGillis, W. R., Gieskes, W. W. C., Klaassen, W., de Groot, H. W., and de Baar, H. J. W.: Fluxes and gas transfer rates of the biogenic trace gas DMS derived from atmospheric gradients, J. Geophys. Res., 109, C08S10, doi:10.1029/2003JC001795, 2004.

Zepp, R. G.: Solar UVR and aquatic carbon, nitrogen, sulfur and metals cycles, in: UV Effects in Aquatic Organisms and Ecosystems, edited by: Helbling, E. W. and Zagarese, H., The Royal Society of Chemistry, London, 137–184, 2003.

Table 1. Sampling information and related physical and chemical properties. MRE-E = Mackenzie River estuary-east channel; MRE-W = Mackenzie River estuary-west channel; MS = Mackenzie Shelf; CB = Canada Basin; BB = Baffin Bay; n.d. = not determined. Zero-meter sampling depths denote bucket samples. The separation of MRE-E and MRE-W from MS is only intended to facilitate discussion in the text. All MRE-E and MER-W stations were actually located on the MS.

Region	Sta.	Cruise	Date	Latitude	Longitude	Sampling depth	Bottom depth	Salinity	T	$a_{cdom,412}$	NO_3^-
			dd-mm-yy	(°N)	(°W)	(m)	(m)		(°C)	(m^{-1})	(µM)
MRE-E	S0	CFL	30-06-08	69.27	134.09	0	1.0	0	n.d.	2.14	3.53
	3	CFL	29-07-08	69.50	133.25	0	3.8	11.1	14.9	1.56	0.51
	391	Malina	16-08-09	70.10	133.54	0	34.6	27.82	3.2	1.23	0.01
	394	Malina	16-08-09	69.85	133.49	0	12.4	21.46	8.8	1.11	0.01
	396	Malina	16-08-09	69.68	133.46	0	6.3	17.27	8.2	0.82	0.12
	398	Malina	16-08-09	69.53	133.42	0	3.1	16.37	8.8	0.13	0.70
	434	CFL	30-06-08	70.18	133.56	2.7	40.0	29.03	3.6	0.28	0.40
MRE-W	691	Malina	13-08-09	69.39	137.79	0	43.7	23.61	5.2	2.04	0.00
	693	Malina	13-08-09	69.30	137.40	0	32.3	15	8.8	1.89	0.63
	694	Malina	13-08-09	69.25	137.20	0	9.0	9.43	9.3	1.66	1.79
	695	Malina	13-08-09	69.20	137.01	0	5.0	7.04	9.3	1.15	2.60
	697	Malina	13-08-09	69.13	136.68	0	1.7	0.15	10.3	0.39	3.62
MS	170	Malina	07-08-09	70.92	128.92	3	35	29.01	3.2	0.20	0.00
	670	Malina	10-08-09	69.80	138.43	3	174	23.5	4	0.33	0.01
CB	320	Malina	09-08-09	71.56	133.96	2.8	1159	26.46	−0.8	0.1	0.01
	640	Malina	11-08-09	70.33	139.10	3.3	564	21.43	2.1	0.24	n.d.
	1526	CFL	03-07-08	72.01	131.33	5	1050	25.47	−0.9	0.17	0.30
	1526	CFL	03-07-08	72.01	131.33	160	1050	33.66	−1.5	0.11	12.1
	1526	CFL	03-07-08	72.01	131.33	950	1050	34.87	0	0.09	12.2
BB	126	SOLAS	18-09-08	77.35	73.42	0	326	31.59	3.1	0.1	0.29
	140	SOLAS	11-09-08	75.04	64.49	0	280	30.88	3.6	0.06	0.05
	303	SOLAS	07-09-08	74.23	89.65	0	228	30.98	0.3	0.05	0.14

Table 2. Fitted $\Phi^*_{dms,\lambda_{ref}}$ and $S_{\Phi^*_{dms}}$ values for Eq. (4) in the text. Also shown are irradiation temperature and $\Phi^*_{dms,330}$ calculated from Eq. (4). R^2 is the coefficient of determination for regression of the predicted DMS photodegradation rate against the measured rate in an irradiation cells (see Sect. 2.4). Keys for the "Region" column are the same as in Table 1.

Region	Station	Irr. T (°C)	$\Phi^*_{dms,\lambda_{ref}}$ [m^3 (mole photons)$^{-1}$]	$S_{\Phi^*_{dms}}$ (nm^{-1})	R^2	$\Phi^*_{dms,330}$ [m^3 (mole photons)$^{-1}$]
MRE-E	S0	2.0	0.30	0.037	0.987	0.07
	3	2.0	0.58	0.039	0.995	0.12
	391	4.0	0.66	0.020	0.982	0.30
	394	4.0	0.37	0.030	0.974	0.11
	396	4.0	0.18	0.021	0.989	0.08
	398	4.0	0.16	0.022	0.970	0.07
	434	2.0	1.19	0.044	0.992	0.20
MER-W	691	4.0	0.36	0.025	0.943	0.14
	693	4.0	0.18	0.014	0.971	0.11
	694	4.0	0.37	0.038	0.980	0.08
	695	4.0	0.10	0.011	0.981	0.06
	697	4.0	0.26	0.034	0.994	0.07
MS	170	4.0	0.96	0.039	0.995	0.20
	670	4.0	0.51	0.019	0.985	0.24
CB	320	4.0	1.27	0.034	0.952	0.33
	640	4.0	0.94	0.032	0.990	0.26
	1526 (5 m)	2.0	2.42	0.063	0.996	0.19
	1526 (160 m)	2.0	6.10	0.051	0.984	0.81
	1526 (950 m)	2.0	18.0	0.061	0.992	1.54
BB	303	2.0	1.57	0.024	0.967	0.60
	140	2.0	0.79	0.010	0.994	0.53
	126	2.0	2.15	0.022	0.993	0.91

Table 3. Photochemical DMS turnover rate constants (k_{dms}) and their corresponding ratios of CDOM to total absorption coefficient, upper mixed layer depths (UMLD), and downwelling solar UV photon fluxes (290–500 nm) just below the sea surface. Absorption coefficients for CFL stations (Sta. S0, 3, and 434) were not measured. The $a_{cdom,330}/a_{t,330}$ ratios for Sta. S0 and 3 were estimated from the best fit of the $a_{cdom,330}/a_{t,330}$ ratio to salinity covering data with salinity ≤ 23.5 ($Y = 0.025X + 0.42$, $R^2 = 0.922$, $n = 10$). The $a_{cdom,330}/a_{t,330}$ ratio for Sta. 434 was assumed equal to that for Sta. 391 based on their similar salinities (see Table 1). Absorption data for the Baffin Bay (Sta. 126, 140, and 303) were obtained from Bélanger et al. (2008). Sta. 1526 refers to surface water (5 m) only. The UMLDs were calculated using the 0.05 kg m^{-3} difference criterion.

	Station	$a_{cdom,330}/a_{t,330}$	UMLD (m)	$Q_{d,0-}$ (mol photons m^{-2} d^{-1})	k_{dms} (d^{-1})
MRE-E	S0	0.42	1.0	18.7	0.039
	3	0.7	3.0	14.3	0.043
	391	0.87	4.0	7.03	0.11
	394	0.92	4.0	5.47	0.026
	396	0.90	4.0	5.47	0.026
	398	0.83	3.1	5.47	0.032
	434	0.87	4.5	19.4	0.059
MER-W	691	0.95	4.0	10.6	0.045
	693	0.78	4.5	10.6	0.048
	694	0.77	4.5	10.6	0.012
	695	0.60	4.0	10.6	0.030
	697	0.35	1.7	10.6	0.014
MS	170	0.66	11.5	10.7	0.010
	670	0.96	10.5	7.60	0.042
CB	320	0.93	12.5	11.2	0.015
	640	0.96	9.5	8.07	0.030
	1526	0.93	19.0	19.3	0.010
BB	126	0.92	12.5	2.00	0.028
	140	0.92	17.5	3.53	0.030
	303	0.92	11.5	3.56	0.023

Table 4. Photochemical DMS turnover rate constants compiled from this study and the literature. Mackenzie Shelf includes MER-E and MER-W in Table 1. UML = upper mixed layer.

| Area	Season	k_{dms} (d^{-1})	Layer	Reference
Mackenzie Shelf	Jun–Aug	0.01–0.11	UML	This study
Canada Basin	Jul–Aug	0.010–0.030	UML	This study
Baffin Bay	Sep	0.023–0.030	UML	This study
Equatorial Pacific	Feb–Mar	0.05–0.15	UML	Kieber et al. (1996)
North Adriatic Sea	Aug–Sep	0.14–0.4	0–20 m	Brugger et al. (1998)
North Atlantic	Jun	0.04–2.5	UML	Simó and Pedrós-Alió (1999)
North Sea	Jun	0.10–0.37	0–20 m	Hatton (2002)
Sargasso Sea	Jul	0.05–0.22	UML	Toole et al. (2003)
Ross Sea	Nov	0.5–0.71	UML	Toole et al. (2004)
Bering Sea	Aug	0.02–0.11	0–20 m	Deal et al. (2005)
Northeast Pacific	Jul	0.03–0.25	UML	Bouillon et al. (2006)
Sargasso Sea	Jul–Aug	0.48–0.6	UML	Gabric et al. (2008)
Ross Sea	Jan	0.037–0.17	UML	del Valle et al. (2009)
Greenland Sea	Jul	0.23–1.05	UML	Galí and Simó (2010)
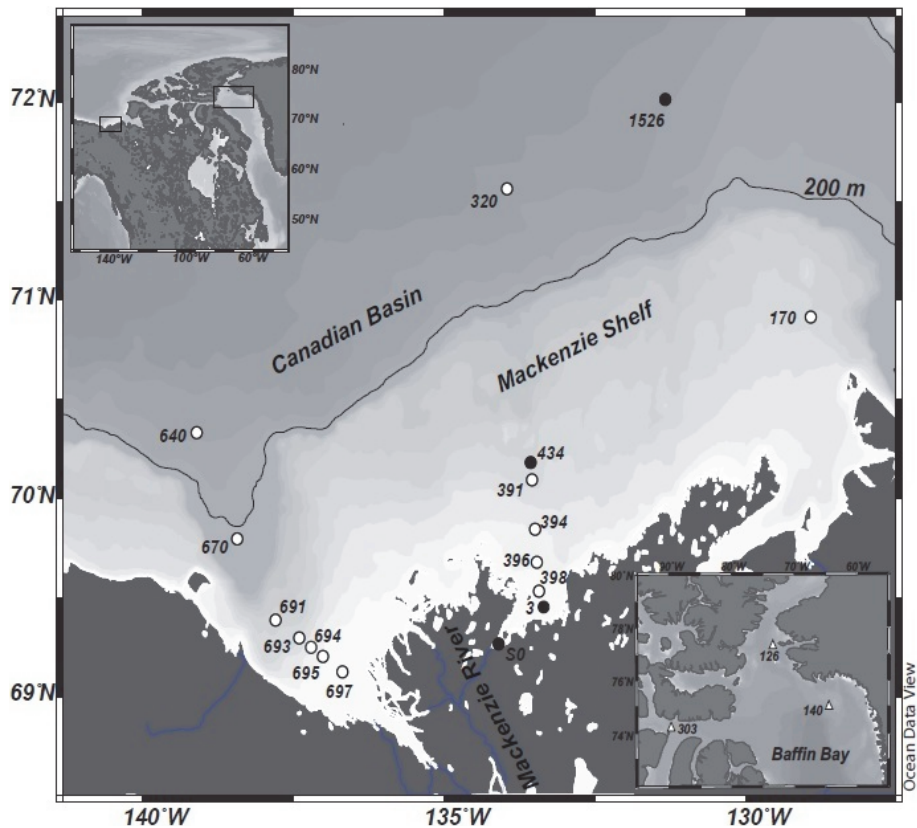
Fig. 1. Sampling map showing the Mackenzie Shelf and Canadian Basin in the western Canadian Arctic and the Baffin Bay in the eastern Canadian Arctic. Open circles denote CFL stations in June and July 2008, closed circles signify Malina stations in August 2009, and open triangles represent SOLAS stations in September 2008.
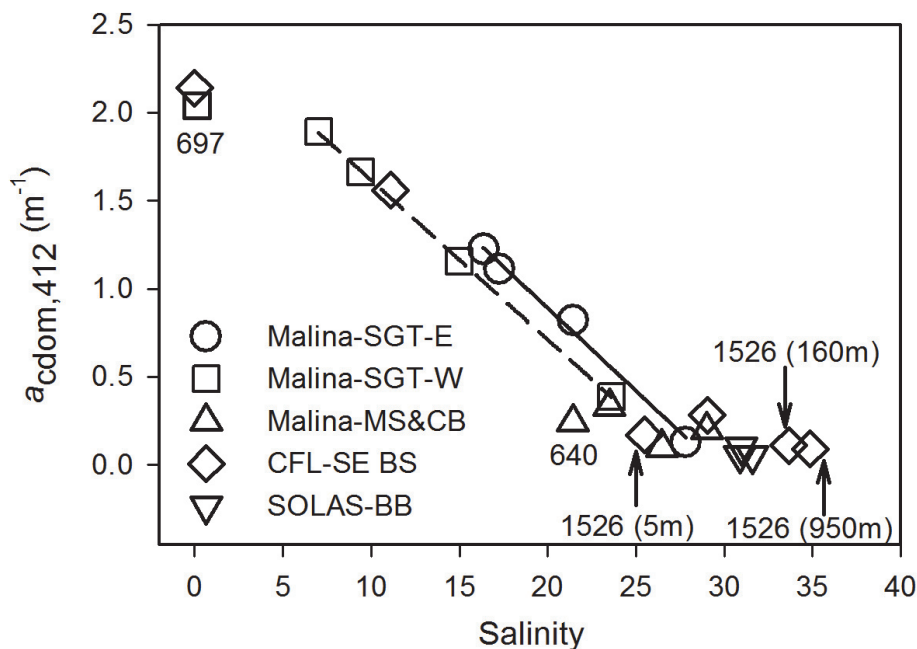
Fig. 2. Scatter plot of CDOM absorption coefficient at 412 nm versus salinity. SGT-E = salinity gradient transect-east channel; SGT-W = salinity gradient transect-west channel; MS = Mackenzie Shelf; CB = Canada Basin; SE BS = southeastern Beaufort Sea (incuding both coastal and open ocean waters); BB = Baffin Bay.
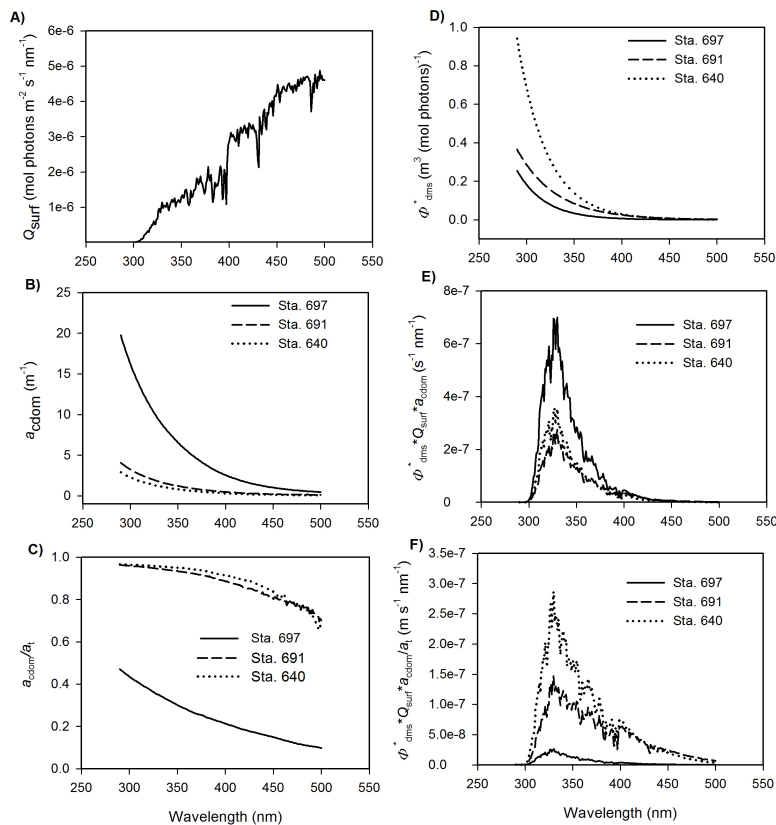
Fig. 3. Surface solar irradiance spectrum (**A**, see definition in Sect. 3.2), examples of CDOM absorption spectra (**B**) and their corresponding CDOM to total absorption ratios (**C**), DMS photolysis AQY spectra (**D**), and surface and water-column DMS photolyis action spectra (**E, F**).
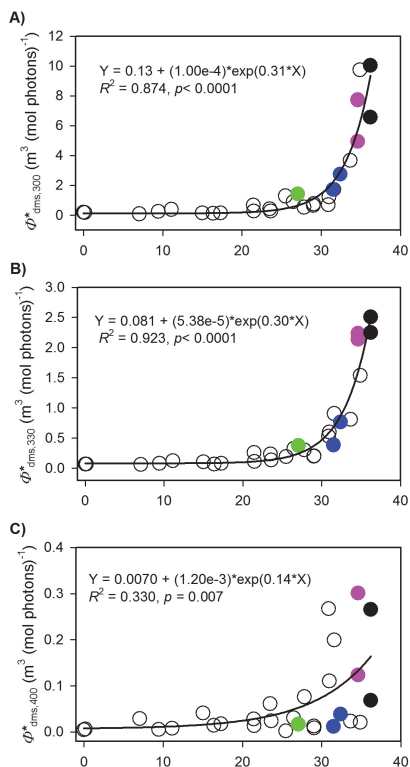
Fig. 4. Scatter plots of DMS photolysis AQY versus salinity for AQY at 300 nm **(A)**, 330 nm (panel **(B)**, and 400 nm **(C)**. Open circles denote data from this study, filled blue circles from the Bering Sea (Deal et al., 2005), filled red circles from the NE subarctic Pacific (Bouillon and Miller 2004, their out-patch values), filled black circles from the Sargasso Sea (Toole et al., 2003). The solid green circles signify data obtained from a sample freshly collected from the lower St. Lawrence estuary off Mont Joli, Quebec (48.5833° N, 68.1833° W). Solid lines are best fits to the data.
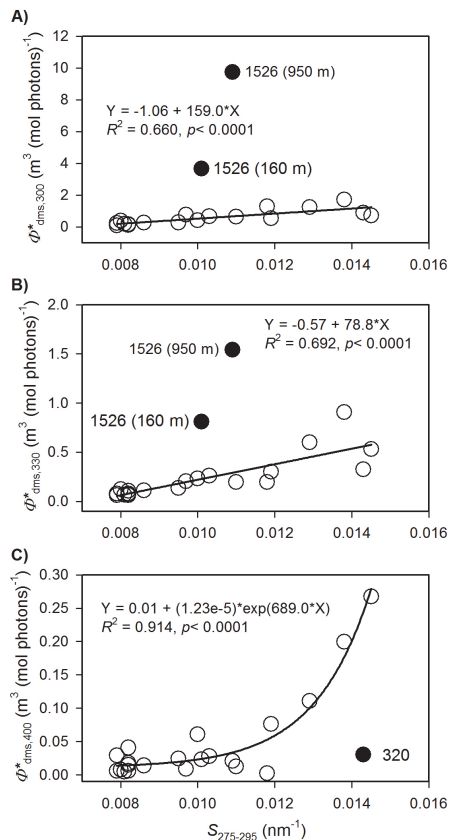
Title Page

Abstract | Introduction

Conclusions | References

Tables | Figures

|◄ | ►|

◄ | ►

Back | Close

Full Screen / Esc

Printer-friendly Version

Interactive Discussion

Fig. 5. Scatter plots of DMS photolysis AQY versus CDOM's spectral slope coefficient (275–295 nm) for AQY at 300 nm **(A)**, 330 nm **(B)**, and 400 nm **(C)**. Solid lines are best fits to the data excluding outliers indicated by filled symbols with station numbers. Spectral slope coefficients were non-linearly computed from the model of $a_{cdom,\lambda} = a_{cdom,\lambda 0} \exp[S \times (\lambda_0 - \lambda)]$ where λ_0 is a reference wavelength.

Title Page

Abstract | Introduction

Conclusions | References

Tables | Figures

Back | Close

Full Screen / Esc

Printer-friendly Version

Interactive Discussion